

# Microstructural Characteristics and Mechanical Properties of an Electron Beam-Welded Ti/Cu/Ni Joint

Feng Zhang, Ting Wang, Siyuan Jiang, Binggang Zhang, and Jicai Feng

(Submitted May 21, 2017; in revised form January 29, 2018; published online April 2, 2018)

Electron beam welding experiments of TA15 titanium alloy to GH600 nickel superalloy with and without a copper sheet interlayer were carried out. Surface appearance, microstructure and phase constitution of the joint were examined by optical microscopy, scanning electron microscopy and x-ray diffraction analysis. Mechanical properties of Ti/Ni and Ti/Cu/Ni joint were evaluated based on tensile strength and micro-hardness tests. The results showed that cracking occurred in Ti/Ni electron beam weldment for the formation of brittle Ni-Ti intermetallics, while a crack-free electron beam-welded Ti/Ni joint can be obtained by using a copper sheet as filler metal. The addition of copper into the weld affected the welding metallurgical process of the electron beam-welded Ti/Ni joint significantly and was helpful for restraining the formation of Ti-Ni intermetallics in Ti/Ni joint. The microstructure of the weld was mainly characterized by a copper-based solid solution and Ti-Cu interfacial intermetallic compounds. Ti-Ni intermetallic compounds were almost entirely suppressed. The hardness of the weld zone was significantly lower than that of Ti/Ni joint, and the tensile strength of the joint can be up to 282 MPa.

**Keywords** electron beam welding, GH600 nickel alloy, microstructure, mechanical property, TA15 titanium alloy

## 1. Introduction

Titanium alloys are the preferred structural materials in the aeronautics and astronautics industries because of their high specific strengths (Ref 1,2). However, their high temperature mechanical properties decrease significantly at operating temperatures above 600 °C (Ref 3). On the other hand, nickel-based alloys can maintain their mechanical properties at elevated temperatures even beyond 1000 °C (Ref 4-6). Therefore, there is an urgent need to join titanium and nickel alloys to reduce the weight and raise the operating temperature of the components.

It has been acknowledged that the traditional fusion welding methods are not feasible for dissimilar metal joints due to the formation of brittle compounds, such as Al/Fe, Ti/Fe and Ti/Ni, that have a detrimental effect on the mechanical properties of the joints and give rise to cracks under thermal stress (Ref 7, 8). According to the Ti-Ni binary phase diagram, many kinds of Ti-Ni intermetallic compounds will form in the weld (Ref 9). For example, Chatterjee et al. (Ref 10) have found brittle NiTi<sub>2</sub> and Ni<sub>3</sub>Ti intermetallic compounds produced in a laser-welded Ti-Ni dissimilar butt joint.

Solid-state joining and brazing methods have been usually used as a viable solution to overcome this difficulty because the base metals can remain solid during these processes. However, it is difficult to successfully apply the solid-state joining methods for nickel and titanium alloys due to the low solubility of nickel in alpha titanium at room temperature. Alemán et al. (Ref 11) reported that a large number of Ti-Ni and Ti-Cr intermetallic phases were produced in the interfaces even for the Ti6242 alloy diffusion-bonded to INCONEL 625 superalloy joints. To restrict the formation of interfacial IMCs, Zuhailawat et al. (Ref 12) selected a 71Ag-28Cu-1 Mg alloy as a filler metal for the spot resistance welding of a titanium/nickel joint. The maximum shear strength at room temperature of the spot-brazed Ti/Ag alloy/Ni joint was much higher than that of a Ti/Ni joint.

Although solid-state joining and brazing methods appear to be promising for solving the problem of brittleness due to the formation of an IMC layer, they are highly limited and are not recommended in some cases. For example, solid-state bonding methods are not applicable for components with complex geometric shapes. Additionally, the components must be heated to elevated temperatures during the diffusion bonding and vacuum brazing process, which is not allowed for some metals. Consequently, a feasible fusion welding method to join these two dissimilar metals is necessary for further development. Electron beam welding is the most frequently used fusion welding technique for joining dissimilar metals because of its advantages such as high energy density, vacuum atmosphere and precise control of heating position and area (Ref 13). Furthermore, a very narrow heat-affected zone can also be produced. Electron beam welding was successfully used for the joining of Ti<sub>3</sub>Al-TC4 titanium alloys (Ref 14) and for the joining of Zr-based BMG to Ni metal (Ref 15). For the joints where an IMC layer is formed, filler metals were usually required for electron beam welding and laser beam welding. Gao et al. (Ref 16) joined Ti6Al4 V titanium alloy and 304L stainless steel by laser beam welding by using a Mg interlayer. As a result, a joint with the tensile strength of 221 MPa was

Feng Zhang, Siyuan Jiang, and Binggang Zhang, Shandong Provincial Key Laboratory of Special Welding Technology, Harbin Institute of Technology at Weihai, 2 Wenhua West Road, Weihai 264209, China; Ting Wang and Jicai Feng, Shandong Provincial Key Laboratory of Special Welding Technology, Harbin Institute of Technology at Weihai, 2 Wenhua West Road, Weihai 264209, China; and State Key Laboratory of Advanced Welding and Joining, Harbin Institute of Technology, 92 Xidazhi Street, Harbin 150001, China. Contact e-mail: fgwangting@163.com.

obtained. The intermetallic compound of  $Mg_{17}Al_{12}$  was observed in the Ti/weld interface, while no intermetallic compound was found in the SS/weld interface. Wang et al. (Ref 17, 18) reported that a crack-free titanium alloy electron beam welded to 304 stainless steel joint was produced by using Cu filler metal, which had a tensile strength of 310 MPa. The weld mainly consisted of Cu solid solution. Only a thin Cu-Ti intermetallic layer was produced in the titanium/weld interface. Tomashchuk et al. (Ref 19) concluded that the insertion of a pure copper interlayer into the electron beam-welded Ti/Fe joint allowed the reduction but not the elimination of the formation of brittle Ti-Fe and Ti-Cr based phases. The local accumulation of Cu-Ti and Cu-Fe-Ti based phases was less detrimental to the strength of the welds, enabling the joining. The thickness of the brittle regions was reduced due to the short lifetime of the melt and was compensated by the toughening effect of the copper solid solution.

Since according to the binary phase diagrams, the chemical reactions in the Ti-Ni couple are similar as those in the Ti-Fe couple, in this paper, a copper filler metal was adopted for the electron beam welding of TA15 titanium alloy and GH600 nickel superalloy. The phase composition, microstructural characteristics and mechanical properties of the joint were analyzed.

## 2. Experimental Procedures

The materials used in the present work were near- $\alpha$  TA15 titanium alloy and GH600 nickel superalloy, both in the rolling state. The chemical composition of TA15 in wt.% was 5.5-7.0 aluminum, 0.5-2.0 molybdenum, 1.5-2.5 zirconium and 0.8-2.5 vanadium with the balance of titanium. The chemical composition of GH600 in wt.% was 0-0.06 carbon, 0-1.0 manganese, 0-0.5 copper, 14.7-17.0 chromium and 6.0-10.0 iron with the balance of nickel. The metals were machined into 50 mm  $\times$  25 mm  $\times$  2.5 mm plates and then mechanically and chemically cleaned. A 0.5-mm-thick pure copper sheet was embedded in the contact face prior to welding. The electron beam was focused on the centerline of the Cu sheet. The welding parameters were selected as follows: accelerating voltage of 60 kV, electron beam current of 18 mA and 20 mA and welding speed of 700 mm/min.

The specimens for microstructure characterization and hardness examination were prepared metallographically and then etched in a reagent of 20 mL  $HNO_3$ , 20 mL HF and 80 mL  $H_2O$ . Microstructure observation on the cross section of the joint was carried out by optical and scanning electron microscopy. The elemental composition was evaluated by SEM-EDS in the spot and line scan modes. X-ray diffraction analysis was carried out to identify the various phases in the joint. The operating voltage was 50 kV, and the current was 25 mA using a Cu target. The scanning range was  $20^\circ$ - $100^\circ$  ( $2\theta$ ) at a rate of  $3^\circ$ /min. Vickers microhardness was measured under a load of 100 g and a dwell time of 15 s. Tensile testing at room temperature was performed to evaluate the joining strength. Three samples were tested to ensure accuracy and repeatability. The specimens were prepared in rectangular bars (50 mm  $\times$  5 mm  $\times$  2.5 mm). The displacement speed was 0.5 mm/min.

## 3. Results and Discussion

### 3.1 Surface Appearances of the Electron Beam-Welded Joints

Surface appearances of the electron beam-welded Ti/Ni joints without and with a copper interlayer directly are shown in Fig. 1. From Fig 1(a), it was clear that cracks can be observed in both the front and back surface, which meant the cracks passed through the whole weld. This phenomenon demonstrated the weldability of TA15 titanium alloy to GH600 nickel alloy was very poor. But when a copper interlayer was embedded in the contact face of Ti/Ni joint, a crack-free joint was obtained. No depression and bulge has been detected in the front and back surfaces. It is proved that the copper interlayer was helpful for the electron beam welding of the Ti/Ni joint.

### 3.2 Microstructural Characteristics

**3.2.1 Microstructural Characteristics of the Electron Beam-Welded Ti/ Ni Joint.** To clarify the reason for the cracking in Ti/Ni weld, microstructure of the cross section of the joint was analyzed as shown in Fig. 2. Figure 2(a) shows that Ti/Ni joint cracked through the weld and cracks were located along the interface between weld and titanium alloy. SEM-EDS was used to further investigate each phase in the weld, and the results are presented in Table 1. The microstructure in the weld near the titanium side is shown in Fig. 2(b). According to the Ti-Ni binary phase diagram (Fig. 3), the microstructure near Ti side as a mixture of  $\alpha$ -Ti and  $Ti_2Ni$  produced by the eutectoid reaction  $\beta-Ti \rightarrow \alpha-Ti + Ti_2Ni$ . Then, in the direction of Ti side to Ni side, the microstructure has turned into the mixture of TiNi and  $Ti_2Ni$  which was caused by the reaction  $L \rightarrow TiNi$  and peritectic reaction  $L + TiNi \rightarrow Ti_2Ni$ . There may be also a small quantity of  $TiCr_2$  among them. Due to the brittleness of intermetallic compounds (IMCs) TiNi and  $Ti_2Ni$ , cracks more easily happened in the phase interface and finally caused the failure of the joint. XRD results on the cracking surface (Fig. 4) also confirmed that the existence of various Ti-Ni IMCs. The microstructure of the central weld zone is shown in Fig. 2(c). The dendritic structure was consisted of IMCs TiNi and  $TiNi_3$  which was caused by the reaction of  $L \rightarrow TiNi + TiNi_3$  which became the base phase. As shown in Fig. 2(d), the microstructure in the weld near Ni side was mostly the solid solution of  $\gamma$ -[Ni, Cr] including three different shapes. There were about 13% element Ti in the  $\gamma$ -[Ni, Cr] (S in Fig. 2d) which was considered as the phase  $TiNi_3$ .

**3.2.2 Microstructural Characteristics of the Electron Beam-Welded Ti/Cu/Ni Joint.** To conclude the function of the copper filler metal on the welding metallurgical process, microstructure of the cross section of the electron beam-welded Ti/Cu/Ni joint were examined in detail as shown in Fig. 5. From the macrostructure of the cross section, it can also be found that no crack emerged in the weld with the assistance of the copper filler metal. Both base metals have been melted, revealing that this was a typical fusion weld. To determine the reason for the successful fusion weld, the microstructure was examined in detail, as shown in Fig. 5(b), (c) and (d). SEM-EDS was used to further investigate each phase in the weld, with the results presented in Table 2. The microstructure in the weld near the titanium side is shown in Fig. 5(b). Based on the different morphologies, this region can be divided into three

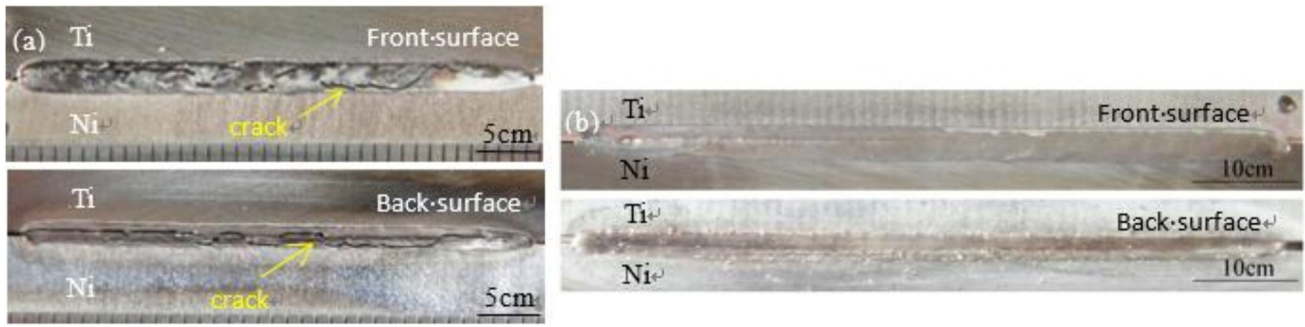


**Fig. 1** Surface appearance of the electron beam-welded Ti/Ni joint (a—without a Cu interlayer; b—with a Cu interlayer)

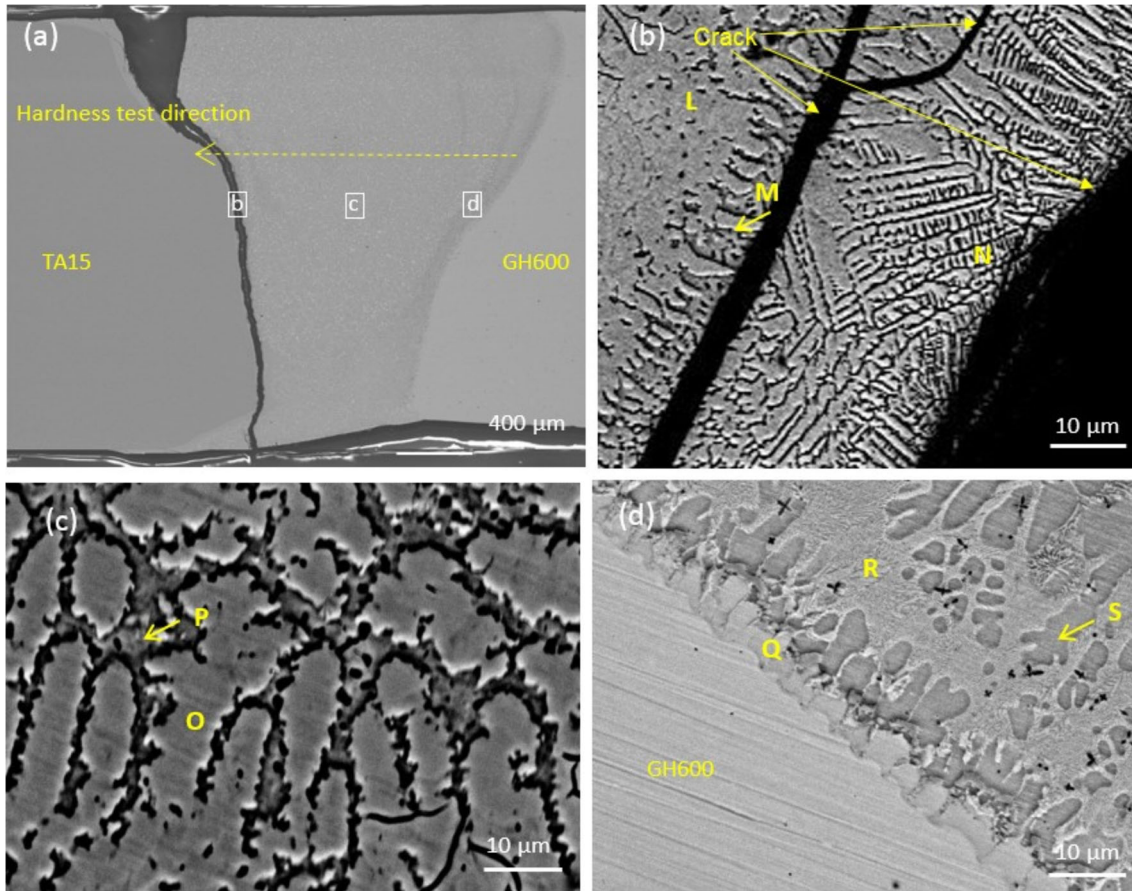


**Fig. 2** Microstructures in different regions of the electron beam-welded Ti/Ni joint (a—cross section, b—weld near Ti side, c—weld center, d—weld near Ni side)

**Table 1** Chemical composition of each phase in Fig. 2 (at.%)

	Fe	Ti	Cr	Ni	Potential phase
L	3	80	7	10	$\alpha$ -Ti + Ti <sub>2</sub> Ni
M	6	76	5	13	$\alpha$ -Ti + Ti <sub>2</sub> Ni
N	2	51	10	37	TiNi + Ti <sub>2</sub> Ni
O	4	30	5	61	TiNi + TiNi <sub>3</sub>
P	2	45	7	46	TiNi
Q	6	14	16	64	$\gamma$ -[Ni, Cr]
R	7	13	17	63	$\gamma$ -[Ni, Cr]
S	2	26	10	62	$\gamma$ -[Ni, Cr] + TiNi <sub>3</sub>



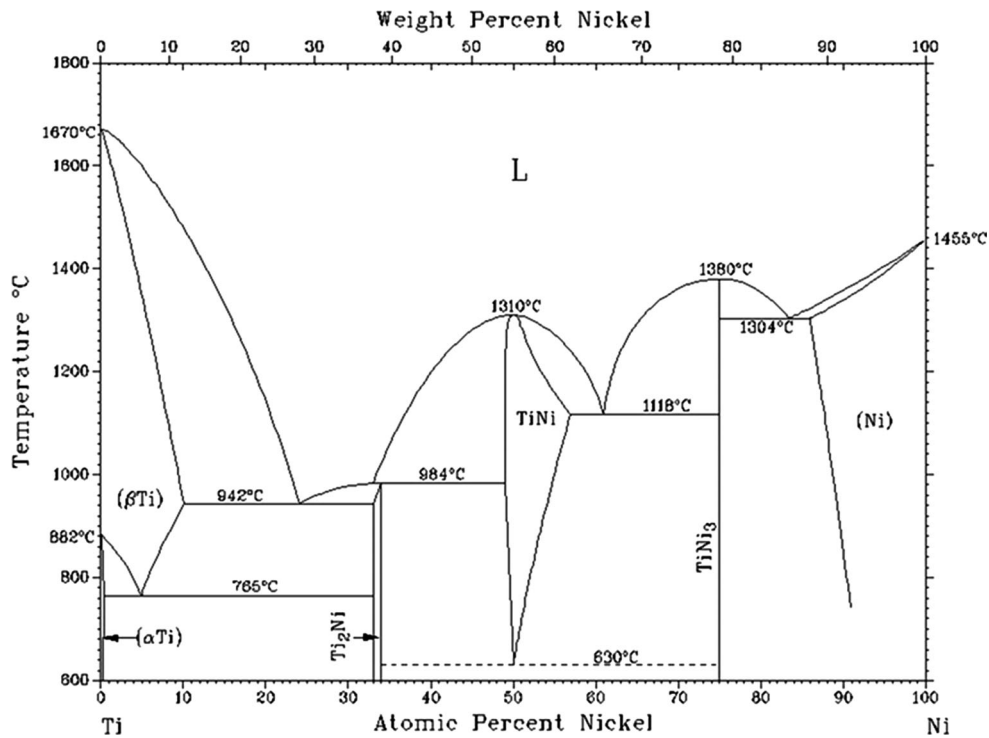


Fig. 3 Ti-Ni binary phase diagram (Ref 20)

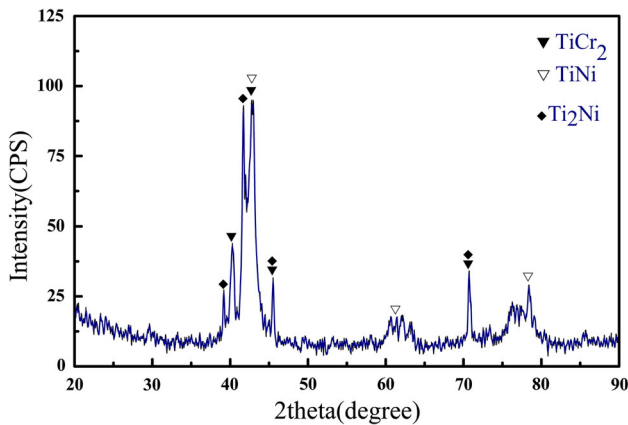
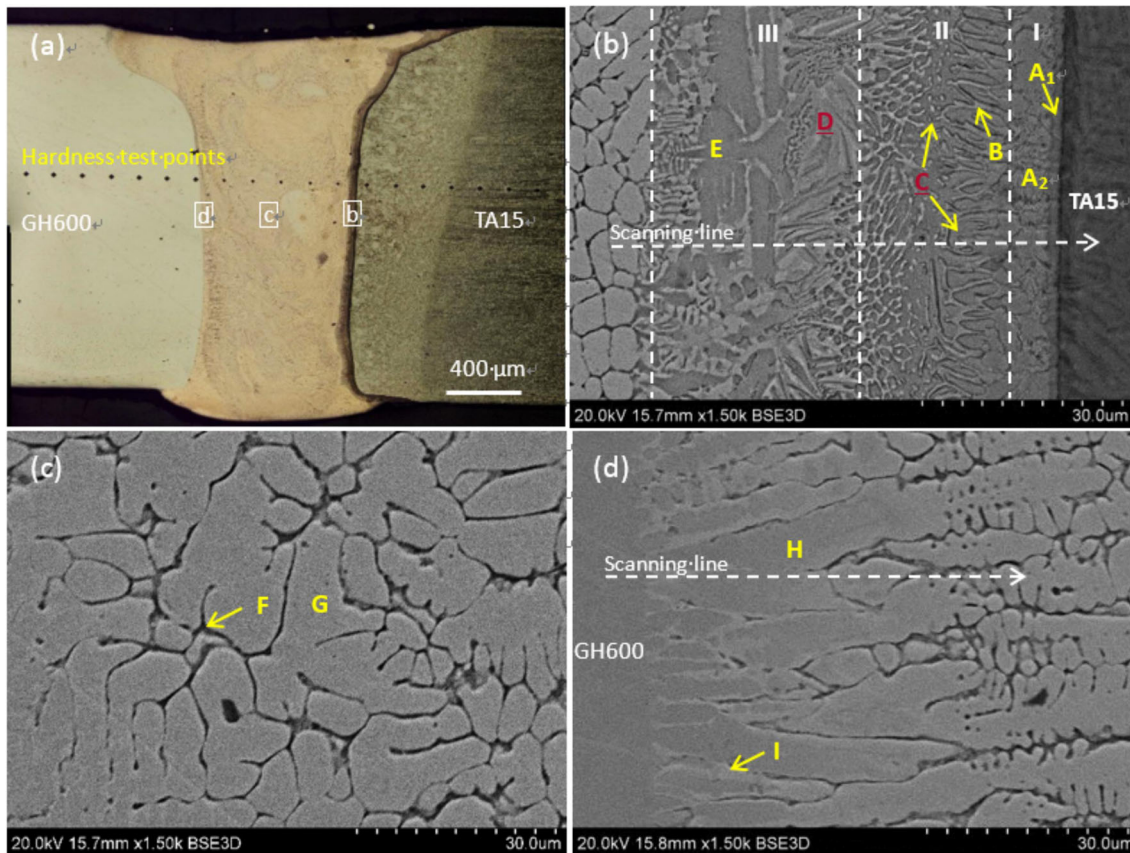


Fig. 4 XRD pattern of intermetallic compound layer of the Ti/Ni joint

zones marked as Zones I, II and III in the figure. The phase constitution in each zone was further analyzed, combining the Ti-Cu binary phase diagram (Fig. 6) (Ref 21) and the Ti-Cu-Ni isothermal section at room temperature (Fig. 7) (Ref 22). Zone I was next to the titanium alloy and consisted of two layers, A<sub>1</sub> and A<sub>2</sub>. Layer A<sub>1</sub> can be recognized as a mixture of  $\alpha$ -Ti and  $\Phi$ -Ti<sub>2</sub>Cu produced by the eutectoid reaction  $\beta$ -Ti  $\rightarrow$   $\alpha$ -Ti + Ti<sub>2</sub>Cu. In layer A<sub>2</sub>, eutectic reaction L  $\rightarrow$  Ti<sub>2</sub>Cu + TiCu occurred at the temperature of 960 °C. Therefore, layer A<sub>2</sub> was a fine eutectic structure containing  $\Phi$ -Ti<sub>2</sub>Cu and  $\phi$ -TiCu. For Zone II, the solidification reaction was more complicated, and it can also be divided into two subzones. The congruent solidification L  $\rightarrow$  TiCu first occurred in Zone II at 985 °C. Then, the peritectic reaction between TiCu (phase B) and the remaining liquid phase produced Cu<sub>4</sub>Ti<sub>3</sub> (Phase C) at 925 °C.

Therefore, Cu<sub>4</sub>Ti<sub>3</sub> was located in the spaces between the TiCu columns in the subzone close to Zone I. Due to the relatively low cooling rate, in the subzone near the weld center, the transformation L + Cu<sub>4</sub>Ti<sub>3</sub>  $\rightarrow$  TiCu<sub>2</sub> (Phase D) could occur at a lower temperature. In this subzone, TiCu<sub>2</sub> assumed a net structure. In Zone III, it consisted of blocky Cu<sub>4</sub>Ti (phase E) and TiCu<sub>2</sub>, produced by the eutectic reaction L  $\rightarrow$  TiCu<sub>2</sub> + TiCu<sub>4</sub> at 875 °C. It should be noted that TiCu<sub>2</sub> is a metastable phase that exists in the temperature range of 890-870 °C. Nevertheless, due to the high cooling rate associated with electron beam welding, it was detected at room temperature in the weld.

For further analysis of the interface structure, EDS line scanning was used to analyze the distributions of the main elements across layers I-III, with the results shown in Fig. 8(a). It can be seen that from the titanium alloy to layer III, the Ti element content fell steeply to 40% at the interface and then gradually decreased to less than 10%. The Cu element content decreased gradually from 70% in layer III to approximately 40% in layer I. The Ni element content remained below 10% in the weld region near TA15. This phenomenon illustrated that the addition of the Cu filler metal can dilute the concentration of Ti and Ni in the weld and impede the migration of Ni from the nickel alloy to the weld near TA15. The formation of Ti-Ni compounds was therefore restrained. The concentration profiles of the major elements across the interface layer also confirmed the continuous distribution of the Ti-Cu compounds formed in the weld zone near TA15 with the thickness of approximately 50  $\mu$ m, which was considered to be harmful to the mechanical properties of Ti/Cu/Ni joint. The XRD pattern of the intermetallic compound layer of the joint (Fig. 9) confirmed the phase composition, and the results were in agreement with the EDS analysis results.



**Fig. 5** Microstructures in different regions of the electron beam-welded Ti/Cu/Ni joint (a—cross section, b—weld near Ti side, c—weld center, d—weld near Ni side)

**Table 2** Chemical composition of the phases in Fig. 5 (at.%)

Element	Ti	Cr	Fe	Ni	Cu	Potential phase
A <sub>1</sub>	77	1	0	2	20	$\alpha$ -Ti + $\Phi$ -Ti <sub>2</sub> Cu
A <sub>2</sub>	52	1	1	5	41	$\Phi$ -Ti <sub>2</sub> Cu + $\varphi$ -TiCu
B	45	2	2	7	44	$\varphi$ -TiCu
C	40	2	2	8	48	$\lambda$ -Cu <sub>4</sub> Ti <sub>3</sub>
D	20	2	2	6	70	Cu <sub>2</sub> Ti
E	17	1	2	8	70	$\eta$ -Cu <sub>4</sub> Ti
F	8	27	5	15	45	[Cu, Cr, Ni]
G	6	4	3	13	74	$\gamma$ -[Cu,Ni]
H	7	5	3	23	62	$\gamma$ -[Cu,Ni]
I	6	4	3	17	70	$\gamma$ -[Cu,Ni]

The microstructure of the central weld zone is shown in Fig. 5(c). Phase G with the dendritic structure was a solid solution of  $\gamma$ -[Cu,Ni], with the solid solution [Cu, Cr, Ni] (Phase F) distributed in its interdendritic regions. Compared to the  $\gamma$  phase, the Cr content in the solid solution [Cu, Cr, Ni] was larger. The Ti element contents in the two phases of this zone were both below 10%, which did not satisfy the conditions for the formation of either Ti-Ni or Ti-Cu compounds. In addition, due to the good plasticity of the copper-based solid solution, the internal stress under a tensile load can be released to a certain extent, improving the joint toughness.

As shown in Fig. 5(d), the microstructure in the weld in the vicinity of the nickel alloy was similar to that in the center of the weld. The solid solution of  $\gamma$ -[Cu,Ni] with a columnar

shape (Phase H) nucleated adjacent to GH600 and grew toward the weld center during the solidification process of the weld pool. Phase I located among the dendritic structures of Phase H was also determined as a  $\gamma$ -[Cu,Ni] solid solution with lower Ni content and greater Cu content.

The concentration profiles of the major elements across the GH600/weld metal interfaces are shown in Fig. 8(b). From GH600 to the weld zone, the Ni content fell steeply at the fusion line and decreased gradually along the direction toward the weld center. At the distance of 25  $\mu$ m to the fusion line, the Ni content was reduced to below 20%. This phenomenon illustrated that the melting amount of GH600 was restricted by the addition of the copper sheet. The majority of the weld zone consisted of copper. The Ti content in this region was also

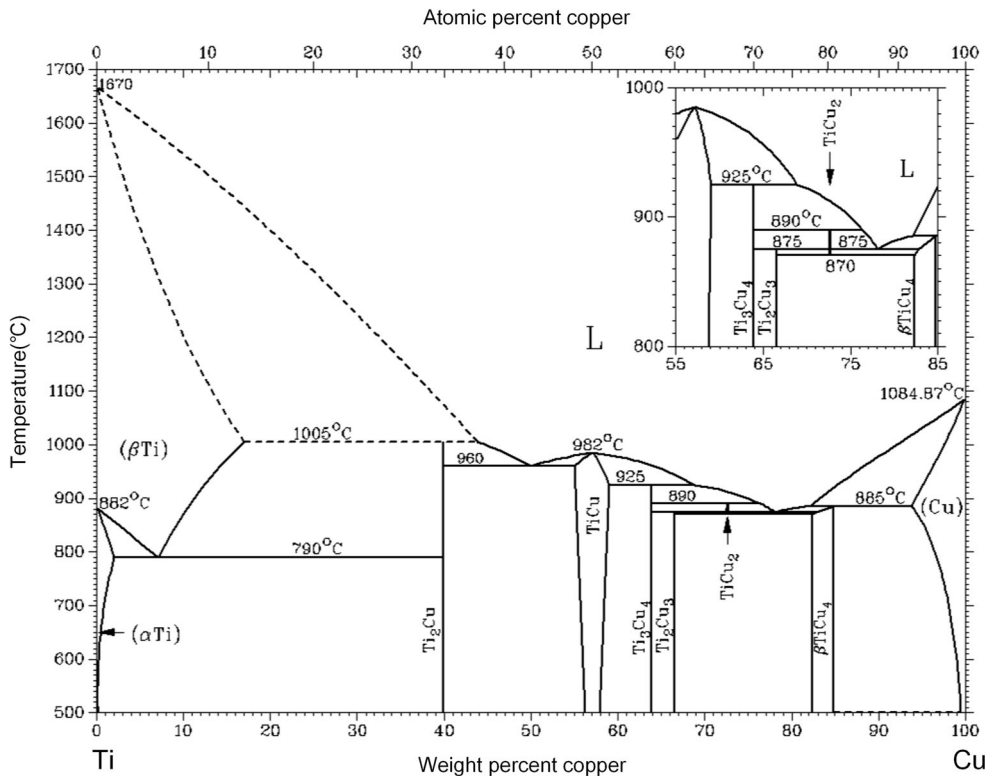


Fig. 6 Ti-Cu binary phase diagram (Ref 21)

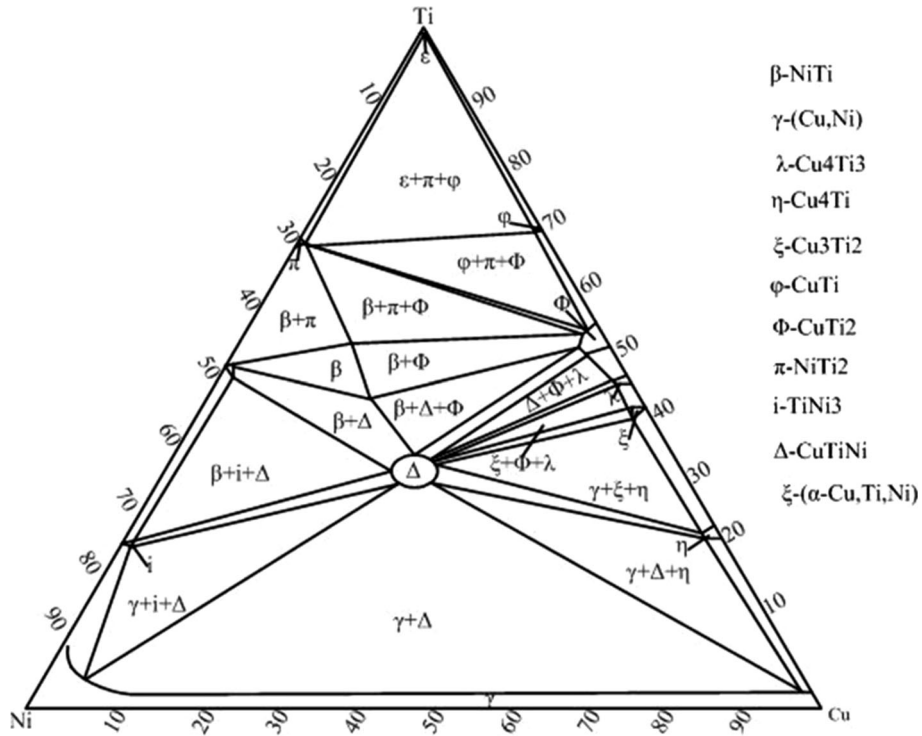


Fig. 7 Ti-Cu-Ni ternary phase diagram (Ref 22)

below 10%, suggesting that Ti migration was very weak and that the formation of Ti-Ni or Ti-Cu compounds in this region was strongly avoided.

Combining the above descriptions, the effect of the copper sheet on the microstructure evolution in the joint can be discussed. Without the addition of the copper filler metal, the

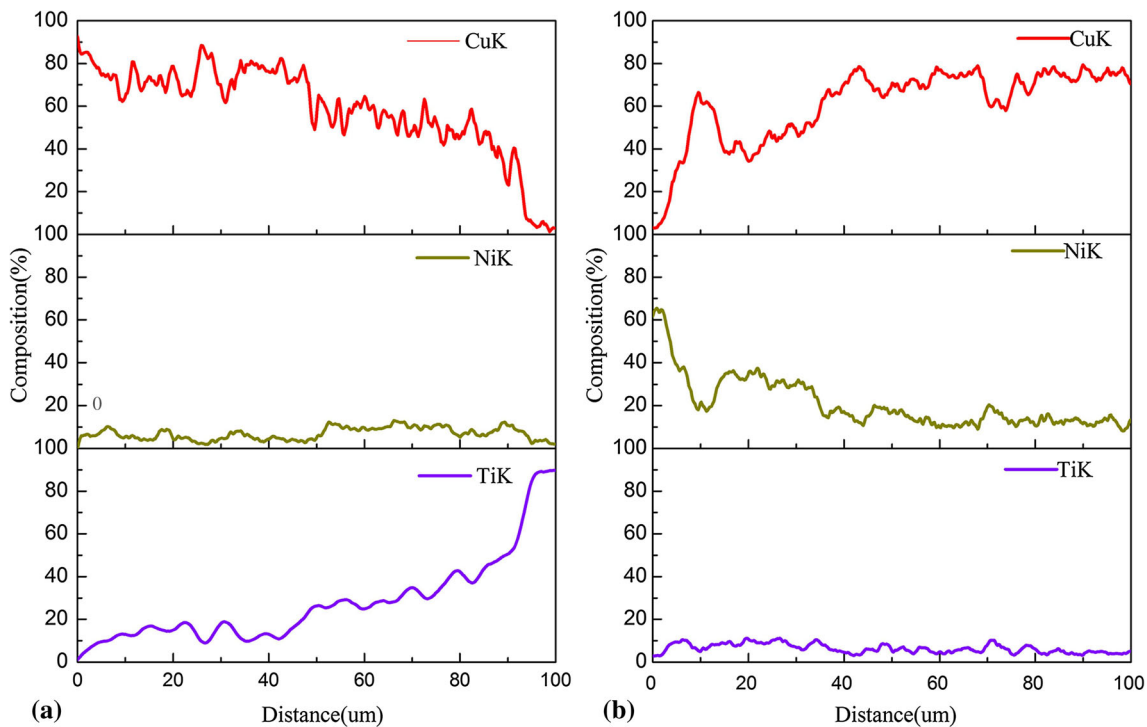


Fig. 8 Element distributions across (a) weld/TA15 and (b) GH600/weld interfaces

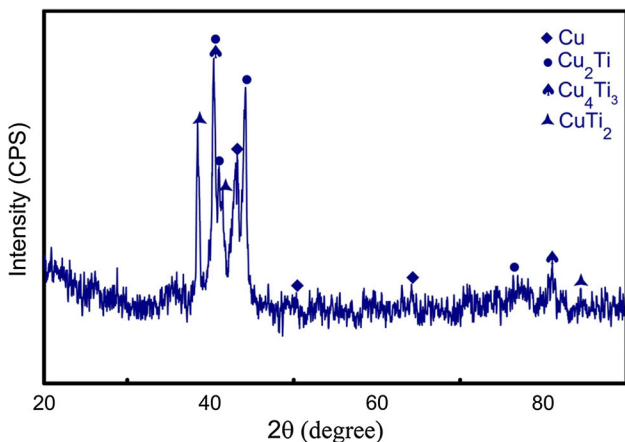


Fig. 9 XRD pattern of intermetallic compound layer of the Ti/Cu/Ni joint

weld would be fully composed of approximately equivalent amounts of Ti and Ni(Cr), which can only exist as intermetallic compounds at room temperature. Since the spot size of the electron beam was fixed, the addition of a copper sheet to the interface reduced the volume of the base metals that was melted. Consequently, the Ti and Ni element fractions in the weld pool decreased. Ultimately, the Ti-Ni compounds were almost completely eliminated. The rest of the weld volume was occupied by a copper-based solid solution. Therefore, the application of the copper filler metal can prevent the formation of Ti-Ni intermetallics in the electron beam-welded Ti/Ni joint.

### 3.3 Mechanical Properties of the Electron Beam-Welded Ti/Ni and Ti/Cu/Ni Joint

Tensile strength of the crack-free joint with a copper interlayer was tested to evaluate the joining quality. The average tensile strength of the joint welded under the beam current of 18 mA reached 282 MPa (max: 298 MPa, min: 272 MPa). It was shown that a certain strength can be obtained for the electron beam-welded TA15/GH600 joint with a copper interlayer, which could provide guidance for the use of the fusion welding techniques for other dissimilar metal joints. It can be seen from the displacement-load curve that the joint fractured with almost no deformation (Fig. 10). The percent elongation was nearly zero, which proved the poor ductility. Cracking surface of Ti/Ni joint in SEM shown in Fig 11(a) implied typical brittle cleavage fracture feature. It can be considered in a quasi-cleavage brittle fracture mode for the Ti/Cu/Ni joint from its crack surface morphology (Fig. 11b). An x-ray diffraction pattern (Fig. 12) of the fracture surface also indicated that cracks are mainly initiated from Zone II near the titanium alloy, namely the mixed zone of  $\text{Cu}_2\text{Ti}$  and  $\text{Cu}_4\text{Ti}_3$ . Therefore, it was concluded that the regions containing the copper-based solid solution show better ductility than the regions consisting of continuous intermetallics.

For a further analysis of the relationship between the microstructure and mechanical properties, the microhardness distribution across the cross section was measured as shown in Fig. 13. Comparing with the hardness of Ti/Ni joint and Ti/Cu/Ni joint, it was clear that the microhardness of Cu-Ti intermetallic was much lower than that of TiNi and  $\text{Ti}_2\text{Ni}$  which can improve the ductility of joint and its crack arrest property. The microhardness in the weld near the nickel alloy and weld center, consisting of a solid solution with supersat-



urated Ti element, was slightly higher than that of the base metal. The microhardness reached the highest value of 540 HV in the Ti-Cu intermetallic layer near the titanium alloy, (similar to the result reported in Ref 17). What is more, with adding the Cu filler metal into the Ti/Ni joint, the solid solution of Ti-Cu was soft and it can deform easily which can relieve the stress at the interface of joint. It can also be deduced that the plasticity of this zone was the poorest. This result was in agreement with the results of the microstructure analysis and the tensile strength test.

Of course, the welding heat input can affect the mechanical property of the joint according to the microstructure. Figure 14 shows the microstructure of the weld at the Ti side under different beam currents observed by optical microscopy. The thicknesses of the IMC layer at three different positions, marked in Fig. 14, were measured as shown in Table 3. And the average obtained values were 66.3  $\mu\text{m}$  and 93.3  $\mu\text{m}$  for the beam currents of 18 and 20 mA, respectively. The heat input increased when the beam current was increased, and as a result, the IMC layer became significantly thicker. Due to the brittleness of the IMCs, a thicker IMC layer corresponded to a lower tensile strength. Therefore, the tensile strength can be further improved by reducing the welding heat input. However, to improve the joint toughness, it is necessary to replace the IMC layer with another element that does not form intermetallics with Cu and Ti, such as vanadium and niobium.

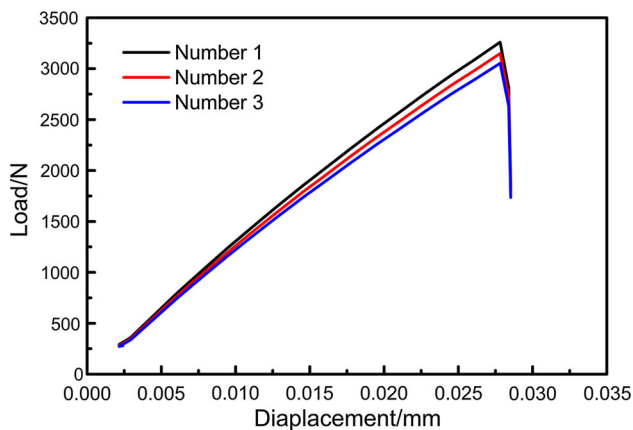


**Fig. 10** Displacement-load curve of Ti/Cu/Ni joint at an 18 mA beam current

## 4. Conclusions

1. Electron beam-welded titanium to nickel joint was not available due to the poor ductility of the joint because of the Ti-Ni IMCs. A crack-free joint of nickel alloy to tita-

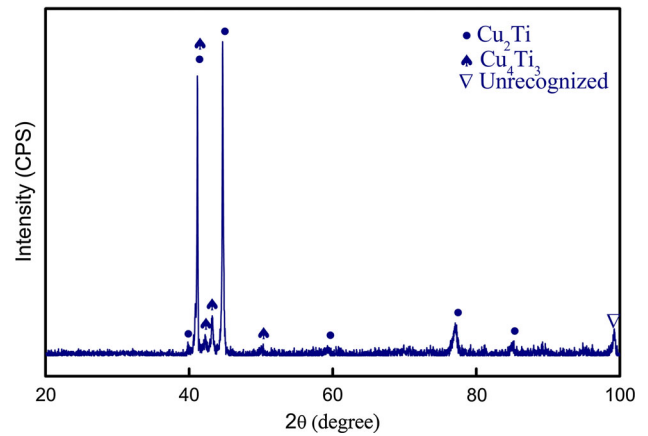


**Fig. 12** XRD pattern of the fracture surface

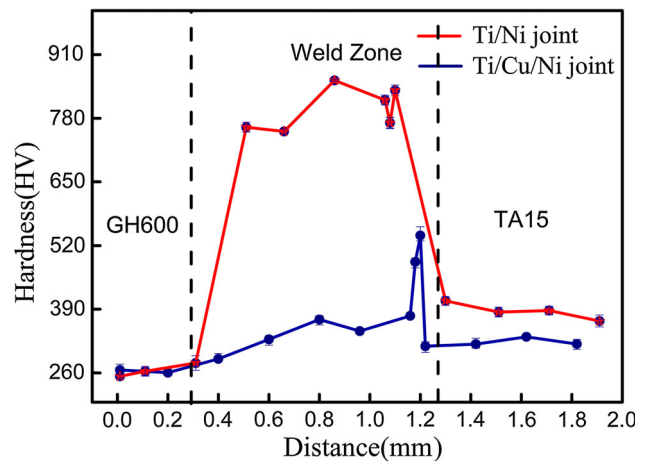


**Fig. 13** Microhardness distribution across the cross sections of the joints

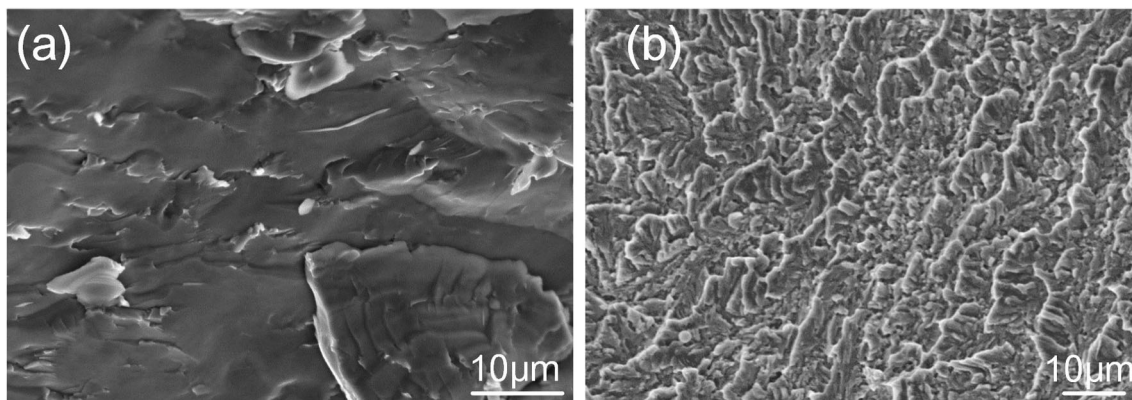


**Fig. 11** Morphology of the cracked surface in the (a) Ti/ Ni joint (b) Ti/Cu/Ni joint



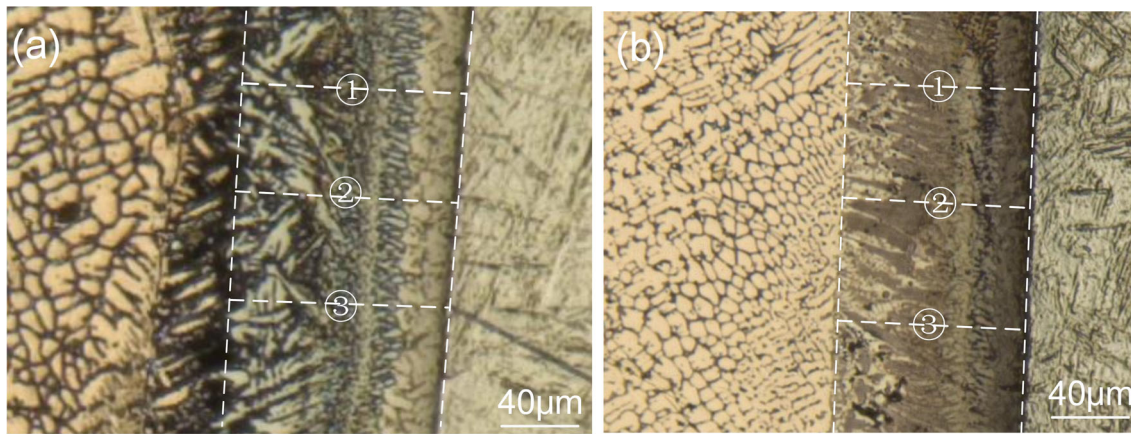


**Fig. 14** Microstructure of the Ti side at different currents (a—18 mA; b—20 mA)

**Table 3** Comparison of the mechanical properties at different currents

Beam current, mA	Thickness of IMCs, $\mu\text{m}$	Tensile strength, MPa	Elongation	Crack position
18	66.3	298	0.06%	Near Ti side
20	83.3	272	0.05%	Near Ti side

nium alloy welded by electron beam welding using a Cu filler metal layer can be obtained. The strength of the joint can reach 282 MPa, and fracture occurred in the Ti-Cu intermetallic compound layer near the titanium side with the brittle fracture mode. The tensile strength of the Ti/Cu/Ni joint was lowered with the increase in the beam current due to the thickening of the IMC layer.

- The weld zone mainly consisted of a [Cu, Ni] solid solution. A Ti-Cu intermetallic compound layer with a thickness of approximately 50  $\mu\text{m}$  was produced in the weld/titanium interface. Ti-Ni intermetallic compounds were not detected in the joint, and only a small amount of ternary  $\Delta$ -CuNiTi intermetallic compounds was produced in the grain boundary near layer III adjacent to the titanium alloy.
- The copper filler metal optimized the mechanical property of the electron beam-welded Ti/Ni joint by reducing the hardness level of the whole weld. The highest hardness of the intermetallic compound layer was lower than that of the Ti-Ni joint. The formation of abundant Cu-based solid solution in the weld could play an important role in stress release and strength improvement.

### Acknowledgments

This work was supported by National Natural Science Foundation of China (51405098) and State Key Lab of Advanced Welding and Joining, Harbin Institute of Technology.

### References

- X.G. Fan, H. Yang, S.L. Yan, P.F. Gao, and J.H. Zhou, Mechanism and Kinetics of Static Globularization in TA15 Titanium Alloy with Transformed Structure, *J. Alloy. Compd.*, 2012, **533**(12), p 1–8
- L. Yang, B. Wang, G. Liu, H. Zhao, and W. Xiao, Behavior and Modeling of Flow Softening and Ductile Damage Evolution in Hot Forming of TA15 Alloy Sheets, *Mater. Des.*, 2015, **85**, p 135–148
- E.O. Ezugwu and Z.M. Wang, Titanium Alloys and Their Machinability—A Review, *J. Mater. Process. Technol.*, 1997, **68**(3), p 262–274
- I. Gurappa, Protection of Titanium Alloy Components against High Temperature Corrosion, *Mater. Sci. Eng. A.*, 2003, **356**(1), p 372–380
- Z. Liu, Q. Bi, Y. Guo, J. Yan, and Z. Yang, Convective heat transfer and pressure drop characteristics of near-critical-pressure hydrocarbon fuel in a minichannel, *Appl. Therm. Eng.*, 2013, **51**(1–2), p 1047–1054
- S.A.P. Li, A. Shyam, R.O. Ritchie, and W.W. Milligan, High Frequency Fatigue Crack Propagation Behavior of a Nickel-Base Turbine Disk Alloy, *Int. J. Fatigue*, 1999, **21**(7), p 725–731
- J. De Keyser, G. Cacciamani, N. Dupin, and P. Wollants, Thermodynamic Modeling and Optimization of the Fe-Ni-Ti System, *Calphad Comput. Coupling Phase Diagr. Thermochem.*, 2009, **33**(1), p 109–123
- H. He, S. Lin, C. Yang, C. Fan, and Z. Chen, Combination Effects of Nocokol Flux with Ni Powder on Properties and Microstructures of Aluminum-Stainless Steel TIG Welding-Brazing Joint, *J. Mater. Eng. Perform.*, 2013, **22**(11), p 3315–3323
- T. Wang, B. Zhang, H. Wang, and J. Feng, Microstructures and Mechanical Properties of Electron Beam-Welded Titanium-Steel Joints with Vanadium, Nickel, Copper and Silver Filler Metals, *J. Mater. Eng. Perform.*, 2014, **23**(4), p 1498–1504
- S. Chatterjee, T.A. Abinandanan, and K. Chattopadhyay, Microstructure Development during Dissimilar Welding: Case of Laser Welding of Ti with Ni Involving Intermetallic Phase Formation, *J. Mater. Sci.*, 2006, **41**(3), p 643–652
- B. Alemán, I. Gutiérrez, and J.J. Urcola, Interface Microstructures in the Diffusion Bonding of a Titanium Alloy Ti 6242 to an INCONEL 625, *Metall. Mater. Trans. A.*, 1995, **26**(2), p 437–446
- H. Zuhailawati, A.M. Saeed, A.B. Ismail, Z. Samad, and A.T. Ariga, Spot Resistance Welding of a Titanium/Nickel Joint with Filler Metal, *Weld. J.*, 2010, **89**(5), p 101s–104s
- Z. Sun and R. Karppi, The Application of Electron Beam Welding for the Joining of Dissimilar Metals: an Overview, *J. Mater. Process. Technol.*, 1996, **59**, p 257–267
- H. Zhang, P. He, J. Feng, and H. Wu, Interfacial Microstructure and Strength of the Dissimilar Joint Ti 3 Al/TC4 Welded by the Electron Beam Process, *Mater. Sci. Eng. A.*, 2006, **425**(1), p 255–259
- J. Kim and Y. Kawamura, Electron Beam Welding of Zr-Based BMG/Ni Joints: Effect of Beam Irradiation Position on Mechanical and Microstructural Properties, *J. Mater. Process. Technol.*, 2008, **207**(1), p 112–117

16. M. Gao, S.W. Mei, Z.M. Wang, X.Y. Li, and X.Y. Zeng, Characterisation of Laser Welded Dissimilar Ti/steel Joint Using Mg Interlayer, *Sci. Technol. Weld. Join.*, 2012, **17**(4), p 269–276
17. T. Wang, B. Zhang, J. Feng, and Q. Tang, Effect of a Copper Filler Metal on the Microstructure and Mechanical Properties of Electron Beam Welded Titanium–stainless Steel Joint, *Mater. Charact.*, 2012, **73**(7), p 104–113
18. B. Zhang, T. Wang, G. Chen, and J. Feng, Contact Reactive Joining of TA15 and 304 Stainless Steel Via a Copper Interlayer Heated by Electron Beam with a Beam Deflection, *J. Mater. Eng. Perform.*, 2012, **21**(10), p 2067–2073
19. I. Tomashchuk, P. Sallamand, H. Andrzejewski, and D. Grevey, The Formation of Intermetallics in Dissimilar Ti6Al4 V/copper/AISI, 316 L Electron Beam and Nd:YAG Laser Joints, *Intermetallics*, 2011, **19**(10), p 1466–1473
20. B. Alemán, I. Gutiérrez, and J.J. Urcola, Interface Microstructures in the Diffusion Bonding of a Titanium Alloy Ti 6242 to an INCONEL 625, *Metall. Mater. Trans. A*, 1995, **26**(2), p 437–446
21. J.L. Murray, The Cu-Ti(copper-Titanium) System, *J. Phase Equilib.*, 1983, **4**, p 81–95
22. P. Villars, A. Prince, and H. Okamoto, *Handbook of Ternary Alloy Phase Diagram*, 1st ed., ASM International, Pittsburgh, 1998